CHIN. PHYS. LETT. Vol. 37, No. 5 (2020) 057501

Origin of Anisotropy in Gadolinium Crystal Using a New Spin Hamiltonian *

Dan Wei(韦丹)[1,2**], Zhibin Chen(陈志斌)[3], Hui Yang(杨慧)[3], Yongjun Cao(曹永军)[3], Chuan Liu(刘川)[4,5]

[1]College of Physics and Electronic Information, Inner Mongolia Normal University, Hohhot 010022
[2]School of Materials Science and Engineering, Tsinghua University, Beijing 100084
[3]College of Physics and Electronic Information, Inner Mongolia Normal University, Hohhot 010022
[4]School of Physics and Center for High Energy Physics, Peking University, Beijing 100871
[5]Collaborative Innovation Center of Quantum Matter, Beijing 100871

(Received 15 December 2019)

Single crystal rare-earth magnets, such as hexagonal-close-packed gadolinium, usually have a large second order anisotropy K_2 and a negative first order anisotropy K_1 at low temperatures, which are difficult to explain using microscopic theories. An atomic scale effective spin Hamiltonian $\mathcal{F}[\{\boldsymbol{S}_i\}]$ is proposed, which, apart from the usual isotropic nearest neighbor coupling J, consists of two new terms that are different for in-plane and out-of-plane neighbors and which are characterized by two new couplings C_1 and C_2, respectively. The hybrid Monte–Carlo method is utilized to sample this system to the desired Boltzmann-like distribution $\exp(-\mathcal{F}/k_{\rm B}T)$. It is found that K_2 and K_1 are compatible with the experimental values and arise naturally from the exchange anisotropy C_1 and C_2, which are less than 0.01% in magnitude of the isotropic exchange energy J. This new model spin Hamiltonian can also be applied to study other magnetic properties.

PACS: 75.30.Gw, 75.10.Hk, 87.10.Rt DOI: 10.1088/0256-307X/37/5/057501

The rare earth magnets usually have a large second order anisotropy K_2 and a negative first order anisotropy K_1 at low temperatures, for both the hexagonal-close-packed (HCP) gadolinium[1] and the tetragonal-structured $Nd_2Fe_{14}B$.[2] For HCP-structured gadolinium, it is known that the effective anisotropy energy $E_{\rm a} = K_1 \sin^2\theta + K_2 \sin^4\theta$, where θ is the angle between the external field and the easy axis. Furthermore, K_1 and K_2 vary significantly with temperature, which is quite different from transition metal magnets. Such an anisotropic magnetic property needs to be understood theoretically. Since gadolinium is a relatively simple rare earth element in terms of structure, it has important applications in magnetocaloric systems as the working material in magnetic refrigeration.[3,4]

Van Vleck pointed out that this magnetic anisotropy originates from the anisotropy of exchange interactions, which bears an extra term of atomic spins compared with the conventional Heisenberg model.[5] Meanwhile, studies have used the density functional theory (DFT) to calculate the anisotropy of Gd from electronic structures; see, for example, Ref. [6]. However, the results of such calculations fail to explain the relevant experiments satisfactorily. In particular, it is difficult to generate a negative K_1 and a positive K_2 at low temperatures. In this work, instead of starting from the electronic structures, we propose a spin Hamiltonian, $\mathcal{F}[\{\boldsymbol{S}_i\}]$, also known as the Landau free energy in the Landau theory, to explain the anisotropic magnetic properties of Gd single crystal. The equilibrium magnetic properties of the system are then obtained by employing the traditional statistical mechanics methods using the canonical ensemble whose partition function reads $Z = \sum_{\{\boldsymbol{S}_i\}} \exp(-\mathcal{F}[\boldsymbol{S}_i]/(k_{\rm B}T))$. We then use Monte Carlo techniques to sample this Boltzmann-like distribution and to obtain the anisotropic constants K_1 and K_2 that are compatible with the experiments.

The hybrid Monte–Carlo (HMC) Hamiltonian of the Gd crystal involves two terms; i.e., the kinetic energy term of atomic spins' conjugate momenta $\{\boldsymbol{\Pi}_i\}$ and the scaled free energy term of atomic spins $\{\boldsymbol{S}_i\}$:

$$\mathcal{H} = \frac{1}{2}\sum_i \boldsymbol{\Pi}_i^2 + \frac{\mathcal{F}[\{\boldsymbol{S}_i\}]}{k_{\rm B}T}, \tag{1}$$

$$\begin{aligned}\mathcal{F} = &-\frac{1}{2}\sum_{\langle i,j\rangle} 2J\boldsymbol{S}_i\cdot\boldsymbol{S}_j + \frac{b}{4}\sum_i \left(\boldsymbol{S}_i^2 - S_0^2(T)\right)^2 \\ &+ \frac{1}{2}\sum_{\langle i,j\rangle}^{\in(xy)} C_1\left(3(\boldsymbol{S}_i\cdot\hat{r}_{ij})(\boldsymbol{S}_j\cdot\hat{r}_{ij}) - \boldsymbol{S}_i\cdot\boldsymbol{S}_j\right)^2 \\ &+ \frac{1}{2}\sum_{\langle i,j\rangle}^{\ni(xy)} C_2\left(3(\boldsymbol{S}_i\cdot\hat{r}_{ij})(\boldsymbol{S}_j\cdot\hat{r}_{ij}) - \boldsymbol{S}_i\cdot\boldsymbol{S}_j\right), \end{aligned} \tag{2}$$

where $\mathcal{H}$, $\{\boldsymbol{S}_i\}$ and $\{\boldsymbol{\Pi}_i\}$ are all dimensionless, and $\mathcal{F}$ is the Landau free energy. The exchange interactions between nearest-neighboring atoms include three terms, the Heisenberg isotropic exchange term, the in-plane (xy) exchange anisotropy energy term with a quartic term in $\{\boldsymbol{S}_i\}$,[7] and the out-of-plane exchange anisotropy term of Van Vleck,[5] with constants J, C_1 and C_2, respectively. A constraint potential which controls the magnitude of an atomic spin in the spin iteration is also introduced in the Hamiltonian[8] with a constant b.

The system is then evolved in a fictitious Monte Carlo time t according to the canonical Hamilton

*Supported by the National Natural Science Foundation of China under Grant Nos. 51771099 and 11621131001.
**Corresponding author. Email: 20188038@imnu.edu.cn
© 2020 Chinese Physical Society and IOP Publishing Ltd

equations:

$$\frac{d\boldsymbol{S}_i}{dt} = \boldsymbol{\Pi}_i, \quad \frac{d\boldsymbol{\Pi}_i}{dt} = -\frac{\partial \mathcal{H}}{\partial \boldsymbol{S}_i}. \tag{3}$$

This set of Hamilton equations will be utilized to generate the configurations of $\boldsymbol{S}_i$ at a certain temperature with the equilibrated distribution $e^{-\mathcal{F}[\{\boldsymbol{S}_i\}]/k_{\rm B}T}$. The HMC method[9] has been numerically extensively used in the lattice field theory community to generate Boltzmann-like distributions. Here we briefly outline the major steps in this algorithm and more details can be found in Ref. [8]. We start from an arbitrary configuration $\{\boldsymbol{S}_i\}$ and give its conjugate momenta $\boldsymbol{\Pi}_i$ from a Gaussian distribution. After descretizing t by steps of δt, Hamilton equations (3) are integrated numerically using the so-called leapfrog integration algorithm for a trajectory length t_0. At the end of each trajectory, the new configuration $\{\boldsymbol{S}_i\}$ is accepted/rejected by the probability $\min(1, e^{-\Delta\mathcal{H}})$ with $\Delta\mathcal{H} = \mathcal{H}(t_0) - \mathcal{H}(0)$. In this way, the desired ensemble of configurations of $\{\boldsymbol{S}_i\}$ is generated.

The HMC model of the Gd crystal is an effective field theory in which the spin $\boldsymbol{S}_i$ is treated as a classical vector. The input parameters include $S_0(T)$ in the constraint potential, and the exchange constants J, C_1, C_2. The 0 K constraint potential parameter is $S_0(0) = 3.55$, which gives a 0 K atomic moment $g_0 S(0)\mu_{\rm B} = 7.1\mu_{\rm B}$ and a 0 K saturation magnetization $M_{\rm s}(0) = 1980\,{\rm emu/cm^3}$ with lattice constants $a = 0.364$ nm and $c/a = 1.588$ of HCP Gd.

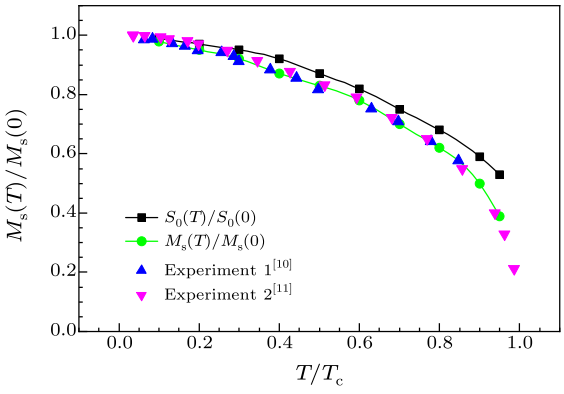

Fig. 1. Simulated scaled saturation $M_{\rm s}(T)/M_{\rm s}(0)$ compared with experiments (exp1[10] and exp2[11]), simulated with $S_0(T)$ in the constraint potential ($b/k_{\rm B}T_{\rm c} = 100$).

To fix the input isotropic exchange J and $S_0(T)$ in the constraint potential, we compare the simulated $M_{\rm s}(T)/M_{\rm s}(0)$ with the existing experiments. Meanwhile, we must make sure that the system remains in the ferromagnetic phase. It is found that when $J/k_{\rm B}T_{\rm c}$ is around 0.1 (where $T_{\rm c} = 293$ K for Gd), the system is in the ferromagnetic phase, i.e., the average magnetization of the simulated region of the Gd crystal does not change much in an external field from 0–2 T. The average magnetization of the system is simply the saturation magnetization $M_{\rm s}(T)$ shown in Fig. 1. It can be seen that the simulated $M_{\rm s}(T)/M_{\rm s}(0)$ fits well with experiments[10,11] of Gd crystal, and the input function $S_0(T)/S_0(0)$ is different from the conventional Brillouin function $B_J(x)$ with $J = 7/2$. This fixes $S_0(T)$ that is then carried over to the following simulations.

The main motivation of this model is to explain the low temperature anisotropy $K_1 < 0$ and $K_2 > 0$ of Gd with $K_2 \simeq 2|K_1|$ in magnitude.[1] This implies that the effective anisotropy energy $E_{\rm a} = K_1 \sin^2\theta + K_2 \sin^4\theta$ does not change much when the external field is within $\theta \leq 45^\circ$ around the c-axis. In the DFT calculation of Gd, it was found that the calculated energy increases drastically from $0 - 45^\circ$, see, e.g., Fig. 1 in Ref. [6]. In our model, if we just use the Van Vleck exchange anisotropy term[5]

$$\Delta V = C_{ij}(2S_{zi}S_{zj} - S_{xi}S_{xj} - S_{yi}S_{yj}), \tag{4}$$

it will be still impossible to explain the K_1 and K_2 of Gd because a large K_2 means that the $P_4(\cos\theta)$ term in the Néel's anisotropy theory[7] is large:

$$w = g_1(r_{ij})P_2(\cos\theta_{ij}) + g_2(r_{ij})P_4(\cos\theta_{ij}) + \cdots \tag{5}$$

We realize that, if we use the Van Vleck exchange anisotropy term for the six out-of-plane nearest neighbors, and add the term that is the squared Van Vleck term (which includes $P_4(\cos\theta)$!) for the six in-plane nearest neighbors, it will be then possible that the slow change of the anisotropy energy $E_{\rm a} = K_1 \sin^2\theta + K_2 \sin^4\theta$ within 45° can be explained. Our simulation indeed verifies this conjecture.

In the simulation, the external field $\boldsymbol{H}_{\rm ext}$ with a magnitude $H_{\rm ext} = 20000$ Oe as in experiment[1] is applied at different angles θ with respect to the c-axis. The simulation results at low temperature are listed in Table 1, where the average quantities are $\bar{\mathcal{F}} = (1/N_{\rm meas})\sum_{n=1}^{N_{\rm meas}} \mathcal{F}$, and the average magnetization along $\boldsymbol{H}_{\rm ext}$ reads

$$\bar{M} = -\frac{1}{N_{\rm meas}} \sum_{n=1}^{N_{\rm meas}} g_0\mu_{\rm B} \sum_i \boldsymbol{S}_i \cdot \boldsymbol{H}_{\rm ext}/(V H_{\rm ext}), \tag{6}$$

where the quantities $\mathcal{F}$ and $\boldsymbol{S}_i$ are the ones at the end of the trajectories, $N_{\rm meas}$ is the total number of measurements; V is the total volume of the simulated $16\times8\times8$ hexagonal primitive unit cells (under 3D periodic boundary conditions applied). In Table 1, the numbers in the parenthesis indicates the error of the quantity in last digit. In this work, we present only the results at low temperatures, $T/T_{\rm c} = 0.05, 0.1$, with the emphasis on illustrating the capability of reproducing the correct K_1 and K_2 energies. In principle, the method is applied to higher temperatures as well albeit with much longer autocorrelation for the algorithm hence much more computer time.

The exchange energy density $E_{\rm ex}$ is defined as the average free energy density $\bar{F}/V$ excluding the Zeeman energy $-\bar{M}H_{\rm ext}$. This will be compared with the well-known result of $E_{\rm a} = K_1 \sin^2\theta + K_2 \sin^4\theta$ for different θ in the following. When the energy is measured in the simulation at different angles, e.g.,

at $\theta = 0, \pi/4, \pi/2$, one could infer the values for K_1 and K_2. In our simulation, we have inspected the energies at five different angles. Apart from the above-mentioned three angles, we have also looked at $\theta = \pi/8$ and $\theta = 3\pi/8$ for consistencies.

Table 1. The number of trajectories $N_{\rm meas}$ in the iteration of the Hamilton equations; the exchange energy density $E_{\rm ex} = \bar{\mathcal{F}}/V + \bar{M}H_{\rm ext}$ in units of $10^6\,{\rm erg/cm^3}$ ($\bar{\mathcal{F}}/V$ excludes the Zeeman energy $-\bar{M}H_{\rm ext}$) at different angles θ between c-axis and the external field. For other parameters, at $T/T_{\rm c} = 0.05$, iteration stepsize $dt = 8.1\times10^{-4}$, $S(T) = 3.532$; at $T/T_{\rm c} = 0.1$, $dt = 9.5\times10^{-4}$, $S(T) = 3.500$.

$\frac{T}{T_{\rm c}}$	$\frac{C_1}{k_{\rm B}T_{\rm c}}$	$\frac{C_2}{k_{\rm B}T_{\rm c}}$	$N_{\rm meas}$	θ	$E_{\rm ex}$
0.05	0	0	2^{16}	0	−36362.76(4)
0.05	0	0	2^{16}	$\frac{\pi}{8}$	−36362.76(4)
0.05	0	0	2^{16}	$\frac{\pi}{4}$	−36362.73(4)
0.05	0	0	2^{16}	$\frac{3\pi}{8}$	−36362.75(4)
0.05	0	0	2^{16}	$\frac{\pi}{2}$	−36362.73(3)
0.05	5.1×10^{-7}	-9.5×10^{-6}	2^{16}	0	−36362.93(3)
0.05	5.1×10^{-7}	-9.5×10^{-6}	2^{16}	$\frac{\pi}{8}$	−36363.02(3)
0.05	5.1×10^{-7}	-9.5×10^{-6}	2^{16}	$\frac{\pi}{4}$	−36362.69(3)
0.05	5.1×10^{-7}	-9.5×10^{-6}	2^{16}	$\frac{3\pi}{8}$	−36362.15(4)
0.05	5.1×10^{-7}	-9.5×10^{-6}	2^{16}	$\frac{\pi}{2}$	−36361.51(3)
0.1	5.5×10^{-7}	-6.5×10^{-6}	2^{18}	0	−35515.82(5)
0.1	5.5×10^{-7}	-6.5×10^{-6}	2^{18}	$\frac{\pi}{4}$	−35515.81(4)
0.1	5.5×10^{-7}	-6.5×10^{-6}	2^{18}	$\frac{\pi}{2}$	−35514.79(5)

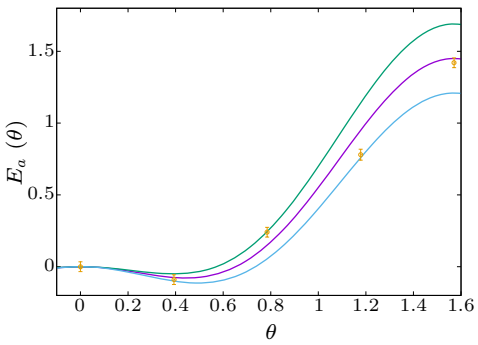

Fig. 2. Simulated $E_{\rm ex}(\theta) - E_{\rm ex}(0)$ (dots) at $T/T_{\rm c} = 0.05$, fits reasonably well with $E_{\rm a}(\theta) = K_1\sin^2\theta + K_2\sin^4\theta$, where K_1 and K_2 are taken from Ref. [1].

At $T/T_{\rm c} = 0.05$, when $C_1 = C_2 = 0$, $E_{\rm ex}$ is isotropic versus angle θ, as seen in Table 1, indicating that both K_1 and K_2 are compatible with zero in this case. However, the anisotropy will appear when C_1 and C_2 are given to be nonzero. In fact, if they are tuned such that $C_1/k_{\rm B}T_{\rm c} = 5.1\times10^{-7}$ and $C_2/k_{\rm B}T_{\rm c} = -9.5\times10^{-6}$, the simulated anisotropy energy density $E_{\rm ex}(\theta) - E_{\rm ex}(0)$ fits well with $E_{\rm a}(\theta)$, as seen in Fig. 2. In this figure, among three curves, the one in the middle is the experimental result of $E_{\rm a}(\theta) = K_1\sin^2\theta + K_2\sin^4\theta$ with $K_1 = -0.85\times10^6\,{\rm erg/cm^3}$ and $K_2 = 2.3\times10^6\,{\rm erg/cm^3}$.[1] The upper/lower curves indicate the errors we obtain for K_1 and K_2 in our simulations that are fed back into the formula of $E_{\rm a}(\theta)$, both having an error of $0.17\times10^6\,{\rm erg/cm^3}$. The data points with errors are the simulated data for $E_{\rm a}(\theta)$ at five different angles which nicely fall into the band around the experimental curve.

At $T/T_{\rm c} = 0.1$, with $C_1/k_{\rm B}T_{\rm c} = 5.5\times10^{-7}$ and $C_2/k_{\rm B}T_{\rm c} = -6.5\times10^{-6}$, $K_1 = -1.0(2)\times10^6\,{\rm erg/cm^3}$ and $K_2 = 2.0(2)\times10^6\,{\rm erg/cm^3}$. It can be seen that the exchange anisotropy constants C_1 and C_2 do vary with temperature, similar to K_1 and K_2.

In conclusion, the rare-earth magnets usually have a large K_2 and a negative K_1 at low temperature. This fact still lacks a microscopic explanation. We propose a spin Hamiltonian $\mathcal{F}[\{\boldsymbol{S}_i\}]$ in Eq. (2) for the HCP gadolinium, with the isotropic Heisenberg exchange being the main term, supplemented by two different exchange terms for in-plane and out-of-plane neighbors characterized by C_1 and C_2. The hybrid Monte–Carlo algorithm is used to study this system. It is found that the experimental values K_1 and K_2 for the anisotropy energy of gadolinium arise naturally when the two parameters C_1 and C_2 are tuned properly. It is also found that the magnitudes of C_1 and C_2 are tiny, several orders of magnitude smaller than the isotropic exchange energy J. We believe that this fact more or less explains why it is extremely difficult to obtain such an effect using DFT-like theories. However, as we show here, anisotropy can show up naturally from our spin Hamiltonian.

The authors would like to thank Professor Tegus at Inner Mongolia Normal University for helpful discussion.

References

[1] Graham Jr. C D 1963 *J. Appl. Phys.* **34** 1341
[2] Drust K D and Kronmüller H 1986 *J. Magn. Magn. Mater.* **59** 86
[3] Brück E 2005 *J. Phys. D* **38** R381
[4] Gschneidner K A and Pecharsky V K 2008 *Int. J. Refrig.* **31** 945
[5] Van Velck J H 1937 *Phys. Rev.* **52** 1178
[6] Abdelouahed S and Alouai A 2009 *Phys. Rev. B* **79** 054406
[7] Néel L 1954 *J. Phys. Radium* **15** 376
[8] Wei D, Song J and Liu C 2016 *IEEE Trans. Magn.* **52** 7100808
[9] Duane S, Kennedy A D, Pendleton B J and Roweth D 1987 *Phys. Lett. B* **195** 216
[10] Elliott J F, Legvold S and Spedding F H 1953 *Phys. Rev.* **91** 28
[11] Nigh H E, Legvold S and Spedding F H 1963 *Phys. Rev.* **132** 1092